Applied Clay Science 231 (2023) 106725

Contents lists available at ScienceDirect

Applied Clay Science

journal homepage: www.elsevier.com/locate/clay

Research Paper

Revealing the manufacturing technology to produce the unique *carreaux de pavement* found in the Iberian Peninsula

Iván Ruiz-Ardanaz *, Marta Gil-Fernández, Esther Lasheras, Adrián Durán *

Department of Chemistry, University of Navarra, Irunlarrea 1, 31008 Pamplona, Spain

ARTICLE INFO

Keywords:
Carreaux de pavement
Mediaeval pottery
Archaeometry
Experimental archaeology
Firing conditions

ABSTRACT

Carreaux de pavement is a type of mediaeval tile common in northwestern Europe, whose method of producing has been unknown until now. In this article, the kiln firing conditions of the unique *carreaux de pavement* found in the Iberian Peninsula were determined by comparing the physicochemical and mineralogical properties of the archaeological tiles with those of some reproductions of the tile's body manufactured in the laboratory (*replica*) made by varying the firing temperature and time, as well as the sample size and thickness. The resistance to acid digestion exhibited by the fired samples was especially revealed. According to the results and the modelling performance with the collected data, it was established that the maximum firing temperature was between 900 and 975 °C, and the time was longer than 24 h. These results show the technology used by mediaeval French potters and are a basis for future studies.

1. Introduction

Humanities fields, such as history, and scientific fields, such as chemistry, are generally perceived as radically different. Traditionally, these two disciplines are considered distinct from each other, even at odds, because of their area of study (Montero et al., 2007; Encyclopaedia of Global Archaeology (EGA), 2022). However, issues that are impossible to solve by only focusing on one branch of knowledge have arisen, making their cooperation vital to move forward. This is the case for archaeometry and experimental archaeology (Montero et al., 2007; Encyclopaedia of Global Archaeology (EGA), 2022). For archaeometry, analytical methods have been applied to obtain more detailed information for the composition of numerous cultural heritage items (Grassi and Quirós-Castillo, 2018). This material characterisation in ceramics solves problems such as the conservation or restoration of said pieces and answers historical questions posed by researchers (Perrin, 2005; Busuttil, 2013). Experimental archaeology has evolved as an exceptionally good way of better comprehending the know-how of other centuries (Ramos, 2004; Gómez-Castañedo, 2005). Hypotheses supported by historical research are tested using scientific techniques and methods, confirming or denying their viability (Ingersoll et al., 1977). Experimental archaeology makes it possible to determine the mode of modelling, configuration of the furnace, type of atmosphere, firing temperature, firing time, etc. (Busuttil, 2013; De Bonis et al., 2017; Bratitsi et al., 2018; Thér et al., 2019; Amicone et al., 2021). The relationship between the paste characteristics and firing procedures is direct. These are described as the series of actions performed by artisans to manufacture ceramic objects from raw clays (Thér et al., 2019; Amicone et al., 2021). To estimate the firing temperatures and times, mineralogical modifications are key features largely described in the literature (Grassi and Quirós-Castillo, 2018; Ramos, 2004; Thér et al., 2019; Amicone et al., 2021).

At the end of the last century, different fragments of tiles, known as *carreaux de pavement*, were discovered in an archaeological intervention in the Castle of Tiebas (Navarre, Spain) (Castiella, 1998; Ramos, 2001). A few years later, part of the original pavement was found in situ in one hall (Ramos, 2009). These *carreaux de pavement* are, due to their typology, unique in the Iberian Peninsula and very different from all other peninsular tiles (Martínez et al., 2011). *Carreaux de pavement* is typical of some mediaeval sites (12th–14th centuries) in northern France and England (Norton, 1992; Mayer and Garrigou, 2000). Determining the manufacturing technology can provide an answer to which technology was used, that of northern France or England, that of the Iberian Peninsula of Islamic tradition, or a combination of both. *Carreaux de pavement* tiles are made up of three layers: paste, slip and glaze. The paste (more commonly called the body) is the thickest layer formed by red clay. The slip is a much thinner layer of white paste that constitutes tile decoration, filling the mould imprint on the body surface and

* Corresponding authors.
E-mail addresses: iruiz.23@alumni.unav.es (I. Ruiz-Ardanaz), adrianduran@unav.es (A. Durán).

https://doi.org/10.1016/j.clay.2022.106725
Received 11 April 2022; Received in revised form 9 September 2022; Accepted 8 October 2022
Available online 20 October 2022

contrasting the body red colour. The glaze is an even thinner layer made of vitreous enamel that provides colour and shine (Barbie et al., 1987; Norton, 1992; Mayer and Garrigou, 2000). Tile workshops used to be located near clay deposits, water sources (for modelling) and wood reserves (for firing) (Norton, 1992). Production began in autumn or winter, when the clay was extracted and left exposed to the environmental elements so that the rain and frost would expose most of the pebbles and impurities (Norton, 1992). Subsequently, the clay was kneaded by stepping on it to make it homogeneous (Norton, 1992). The clay was spread by filling in a square frame 3 cm thick with one side a few centimetres longer than the final tiles (10% shrinkage) (Norton, 1992; Mayer and Garrigou, 2000). To avoid adhesion of the clay to the worktable, a thin layer of sand or ash was spread (Barbie et al., 1987; Norton, 1992; Mayer and Garrigou, 2000). Once the frame was removed, it was left on a smooth surface for the first drying step (Barbie et al., 1987; Norton, 1992). After 24 h or more, tiles destined to be dichromatic were stamped with a mould. For all tiles, the lateral edges were cut with a knife, leaving them slightly bevelled (Barbie et al., 1987; Norton, 1992; Mayer and Garrigou, 2000). The stamped copies were covered with a layer of white clay and water at a 1:2 ratio, filling in the negative left by the mould (Norton, 1992; Mayer and Garrigou, 2000). After a second drying step, the excess white clay was removed by brushing (Norton, 1992; Mayer and Garrigou, 2000). A surface glaze was applied as a mixture of Pb-based compounds diluted in water and applied to the surface of monochromatic and dichromatic tiles with a brush (Norton, 1992; Mayer and Garrigou, 2000). They were then left to dry before firing (Barbie et al., 1987; Norton, 1992; Mayer and Garrigou, 2000). Firing began at a low temperature during the first hours to facilitate the elimination of the remaining moisture in the tiles (Norton, 1992). Subsequently, the temperature was increased to ca. 1000 °C, with the aim of melting the glaze (Norton, 1992). Firing lasted for two days (Norton, 1992). Then, the kiln was allowed to cool slowly (Norton, 1992). Some more recent archaeometric investigations on *carreaux de pavement* estimate that the firing temperature must have been limited to 850–900 °C due to the presence of gehlenite (Ben Amara et al., 2005) and above 800 °C for melting glazes (Cicuttini et al., 2007; Cicuttini et al., 2008) or approximately 1000 °C (Rouzeau et al., 2013).

Detailed study of the original manufacturing technique of *carreaux de pavement* is a pending task for archaeometry. It would be especially interesting to study the set of tiles found in the Iberian Peninsula to determine if the artisans followed the manufacturing technology in France (Barbie et al., 1987; Norton, 1992; Mayer and Garrigou, 2000; Ben Amara et al., 2005; Cicuttini et al., 2007; Cicuttini et al., 2008; Rouzeau et al., 2013) or if some changes were introduced. This paper aims to completely elucidate the firing conditions (temperatures and times, mainly) employed to manufacture Tiebas' Castle's *carreaux de pavement* bodies. With this purpose, archaeometry characterisation of a set of mediaeval tiles located in the castle is applied, as well as experimental archaeology, by reproducing samples (named *replicas*) with different shapes and thicknesses made from a clay similar to that used in the archaeological tiles and heated under different experimental conditions.

2. Materials and analytical methods

2.1. Materials

Eighteen samples of *carreaux de pavement* fragments from Tiebas' Castle from the 13th century were selected for the study (Fig. 1) (Ruiz-Ardanaz et al., 2021). Half of them were monochromatic (without slip-based decoration), and the other half were dichromatic (with slip-based decoration). One-third of the fragments were found in situ on the pavement of the north hall of Tiebas' Castle (Fig. S1). Another third was found in a landfill near the castle (very possibly coming from the north hall pavement after a fire happened in 1377). The remaining third was found on the surface, in the surroundings of the castle, out of strata and archaeological context.

A decalcified clay deposit near Tiebas' Castle was used as the source

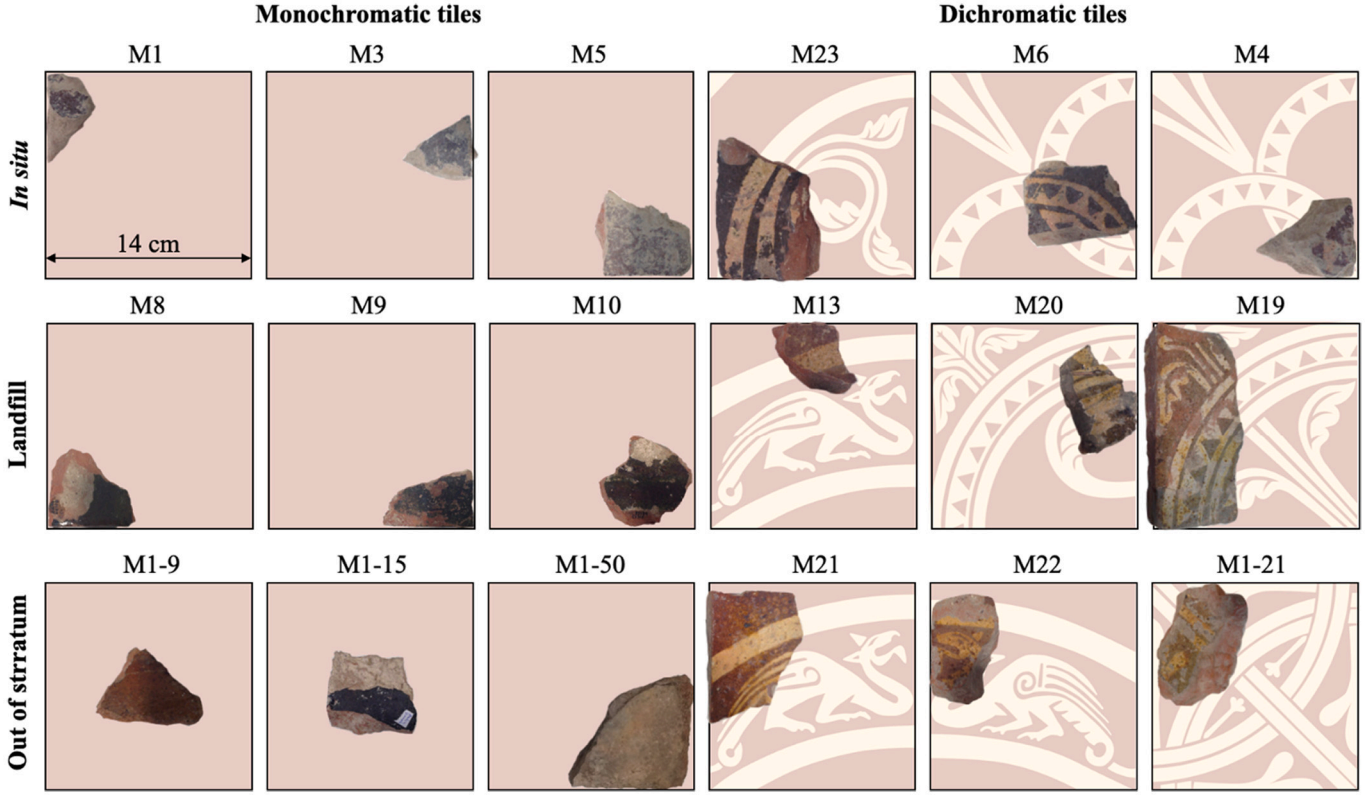

Fig. 1. Analysed tile fragments of *carreaux de pavement* from Tiebas' Castle.

of the raw material for the *replica* samples made for experimental archaeology. This clay (named A15) was chosen among many others according to its elemental and mineralogical composition criteria, which were similar to the archaeological samples (Ruiz-Ardanaz et al., 2021; Ruiz-Ardanaz et al., 2023). Other arguments in favour of using this clay were the proven roaming of tile artisans in the 13–14th century and their knowledge regarding the manufacture of *carreaux de pavement* (González-Martí, 1952; Mayer and Garrigou, 2000; Cicuttini, 2012), prior identification by decalcified clay as the raw material with which the tile pastes were made (Ruiz-Ardanaz et al., 2021), and the proximity to the castle (Fig. 2).

The decalcified clay used (A15) has an elemental and mineralogical chemical composition very similar to that of the tile pastes. Table 1 shows the average elemental composition of tile bodies (18 samples) and A15 clay (5 samples). Both are mainly composed of compounds based on silicon, aluminium and iron and a low content of calcium and magnesium (Ruiz-Ardanaz et al., 2021).

Most of the mineral phases present in both carreaux de pavement and A15 are common, even without the A15 clay being fired. The A15 samples were analysed by XRD once dried at room temperature. The composition of both is based on quartz (SiO_2), illite ($(K,H_3O)(Al,Mg,Fe)_2(Si,Al)_4O_{10}[(OH)_2,(H_2O)]$), haematite ($Fe_2O_3$), calcite ($CaCO_3$) and rutile ($TiO_2$), although the intensity of the reflections depended on the heating temperature (Fig. S2). The presence of calcite in tile bodies is due to a decarbonation reaction during firing and a subsequent recarbonation process (secondary calcite) (Ruiz-Ardanaz et al., 2021).

Table 1
Composition of the tile bodies and the selected clay (A15), obtained by XRF. The results are expressed as the mean ± standard deviation (SD).

	Carreaux de pavement ($n = 18$)	A15 ($n = 5$)
SiO_2	73.4% ± 0.8%	74.2% ± 0.9%
Al_2O_3	16.0% ± 0.6%	16.3% ± 0.5%
Fe_2O_3	3.8% ± 0.2%	4.1% ± 0.2%
K_2O	3.2% ± 0.2%	2.66% ± 0.05%
CaO	1.2% ± 0.5%	1.1% ± 0.3%
MgO	1.2% ± 0.1%	1.1% ± 0.2%
TiO_2	0.54% ± 0.03%	0.51% ± 0.02%

Table 2
Experimental firing temperature and time conditions for the *replica* samples.

	Firing time (h)					
Temperature (°C)	1	3	6	24	48	72
700	QP	QP	QP	QP, CU	QP	QP
800	QP	QP	QP	QP, CU	QP	QP
850	QP	QP	QP	QP, CU	QP	QP
900	QP, CU	QP, CU	QP, CU	QP, CU	QP, CU	QP, CU
950	QP	QP	QP	QP, CU	QP	QP
1000	QP	QP	QP	QP, CU	QP	QP
1100	QP	QP	QP	QP, CU	QP	QP

2.2. Methods

Two types of *replica* samples were made to simulate the body of the original tiles: samples with a quadrangular prism shape (denoted QP) and dimensions of 2.5 × 2.5 × 1 cm and samples with a cubic shape (denoted CU) and dimensions of 2.5 × 2.5 × 2.5 cm (this is approximately the width of the archaeological tiles). *Replica* samples were moulded by moistening powdered clay A15. These *replica* samples were dried first at room temperature and then in a drying oven (JP Selecta) at 100 °C for two days. Afterwards, the samples were heated at different temperatures (700, 800, 850, 900, 950, 1000 and 1100 °C) for different times (1, 3, 6, 24, 48 and 72 h) in a Hobersal MOD 12 PR/300 kiln (Table 2). All the firing processes were carried out by heating from room temperature to 500 °C at a ramp rate of 12 °C·min^{-1}, holding at 500 °C for half an hour, increasing the temperature to 700 °C with a ramp rate of 12 °C·min^{-1}, holding for half an hour, and finally increasing the temperature to the final temperatures (700°, 800°, 900°, 950°, 1000°, and 1100 °C) and holding for 1, 3, 6, 24, 48 and 72 h. Cooling was carried out by allowing the kiln to cool down naturally. As mentioned above, the objective was to analyse how the firing conditions affected the physical and mineralogical properties depending on the shapes (QP and CU) of the *replica* samples. QP samples were used to simulate the surface part of the tile body (minor thickness of 1 cm), while in the case of the CU samples, only the innermost area (approximately 2 cm^3) was used to simulate and study the centre of the tile body.

The *replica* samples heated at different temperatures for different times were analysed after grinding in an agate mortar and measured by

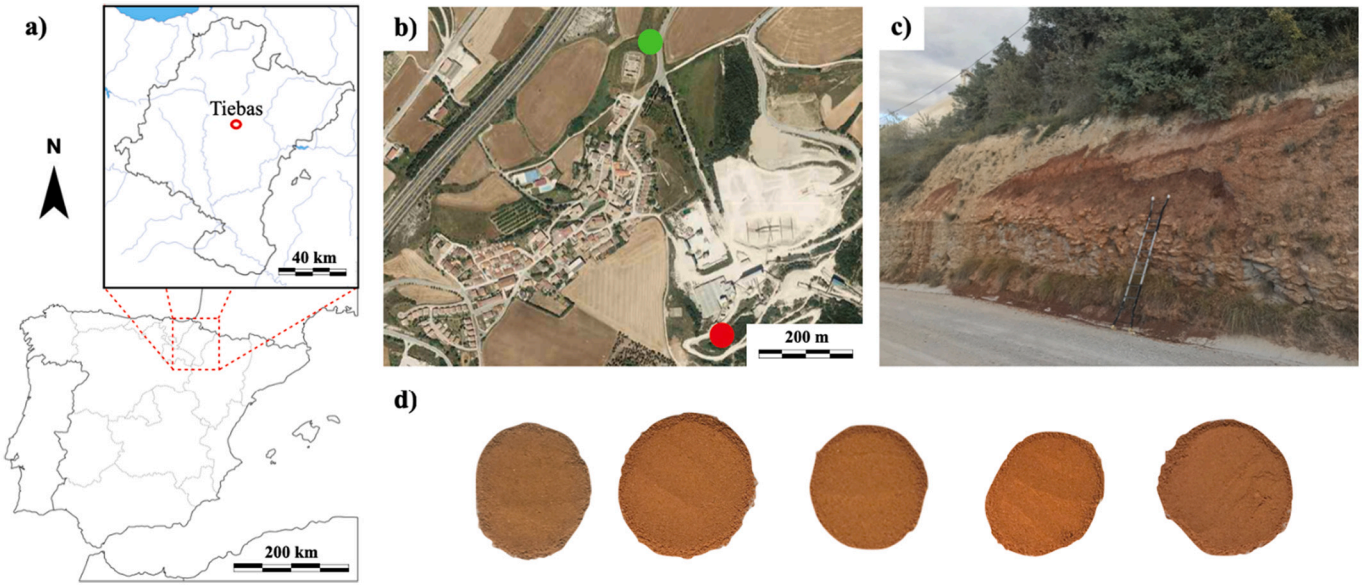

Fig. 2. (a) Location of Tiebas within Navarra and Spain. (b) Location of Tiebas' Castle, in green, and the decalcified clay deposit, in red. (c) Image of the decalcified clay deposit. (d) Decalcified clay samples (5 are shown). (For interpretation of the references to colour in this figure legend, the reader is referred to the web version of this article.)

colorimetry, infrared spectroscopy (FTIR) and X-ray diffraction (XRD). Colorimetric analysis was performed with a CM-2300d Konica Minolta portable colorimeter with a xenon lamp (D65). For all the experiments, the CieL*a*b* colour parameters were measured in triplicate. To obtain the infrared spectra of the sample powders, FTIR Shimadzu IRAffinity-1S equipment with an attenuated total reflectance (ATR) Golden Gate accessory was used. The device consisted of a high-energy ceramic light source and a high-sensitivity DLTGS detector. Spectra were acquired with 100 scans and a resolution of 4 cm^{-1}, with 100 scans in each measurement and a wavenumber interval of 4000 to 600 cm^{-1}. For X-ray diffraction experiments, Bruker D-8 Advance ECO equipment was used; the diffractometer used a Cu anode. The detector was a LYNXEYE XE-T detector, and experimental data were collected in the 2θ range of 5° to 70° with a step size of 0.02° and 1 s per step. The intensity counts of each diffractogram have been normalised with respect to the maximum reflection of the quartz at $2\theta = 26.6°$ (PDF 33–1161). The limit of detection (LOD) and limit of quantification (LOQ) of the XRD intensities values have been established as the mean background values plus 3 or 10 standard deviations, respectively. In order to comparatively assess whether the crystal size of some minerals varies as a consequence of chemical reactions associated with the firing conditions, the crystal size of some samples' phases has been determined with the Scherrer equation:

$$\text{Cristal Size} = \frac{K\,\lambda}{\beta\,cos\,\theta} \quad (1)$$

The width at half height of the peak (**β**) in the reflection of greatest intensity has been used in the Scherrer equation (X-ray wavelength (**λ**) = 1.5406 Å; dimensionless shape factor (K) = 0.89) to obtain the mineral crystal size. Comparisons with archaeological samples were performed. These samples were measured by using the same analytical techniques and the same conditions.

As an exploratory analysis, the diffractograms have been analysed by means of PCA (Principal Component Analysis) with the aim of carrying out a more objective identification of the mineral phases that were modified with the firing temperatures or firing times. The PCA identifies which are the linear combinations of the experimental data and orders the linear combinations according to their variability (Ramis-Ramos and Álvarez-Coque, 2001). In this sense, a data matrix (X) was built considering the counts or intensities of the reflections (each Bragg angle) as variables. The PCA has been applied to different sets of results. Each set of results was made up of diffractograms data from replicas with the same shape (QP or CU) and with the same firing temperature (eg 900 °C) or with the same firing time (eg 24 h). The intensity data were normalised according to the sample and according to the Bragg angle. PCA analysis was applied to this matrix, obtaining: a matrix of scores (U), a matrix of coefficients (*V*) and the % of variability that explains each Principal Component (Ramis-Ramos and Álvarez-Coque, 2001). The scores matrix (U) allowed to evaluate if the results of the two main components (C1 and C2) followed a trend proportional to firing temperatures or firing times. The matrix of coefficients allowed to identify which were the reflections (Bragg angles) with the greatest variability.

To evaluate the chemical stability of the samples after firing, they were attacked with aqua regia (HNO_3:HCl 1:3) in a microwave digester. Strong acids such as hydrochloric and/or nitric acids are capable of solubilizing some metal oxides, like iron oxides, unable to solubilize by using other acids. However, these strong acids are not capable of solubilizing minerals such as quartz, other silicoaluminates or titanium oxides. The possibility of eliminating some major components and keeping others intact opens the possibility of evaluating the ceramics internal structure. A total of 0.250 g of both archaeological and experimental powder samples (*replicas*) was weighed in duplicate in Teflon tubes. Afterwards, 12 mL of aqua regia was added. Samples were then subjected to treatment in a microwave digester (MarsXtraction MarsXpress) at 180 °C for 15 min and then at 210 °C for 50 min. The power applied in the microwave digester was 1600 W. The supernatant liquid and solid residue were separated by centrifugation at 1500 rpm for 15 min. The solid residue was washed successively for acid removal, left to dry in a drying oven and analysed by colorimetry and X-ray fluorescence (XRF). For XRF, samples were analysed with a 4 μm polypropylene filter in a He atmosphere with Bruker S2 Puma equipment (X-ray tube with a silver anode). Quantification was performed with *Spectra Results Manager* software. To comparatively estimate the compressive strength of the CU samples, they were subjected to compression in a Perkin Elmer hydraulic press with a compression rate of 2000 $N{\cdot}s^{-1}$.

3. Results and discussion

3.1. Colorimetry

The colour of a ceramic body is an initial indicator of its heating conditions. Its colour depends on many factors, such as elemental and mineral composition of the bodies, as well as technical factors for manufacturing, such as the atmosphere, thickness, temperatures or times of firing. In all the *replica* samples employed in this paper, the raw material used was the same (A15 clay), so the colour changes must be due to technical factors. Very possibly, the reddish colour of the studied tile body comes from firing in an oxidising atmosphere, as evidenced by the presence of haematite (Ruiz-Ardanaz et al., 2021).

Visually, the colour of most of the *replica* ceramic samples was similar to that of the archaeological mediaeval samples found in Tiebas (Fig. S3).

Regarding the samples used to simulate the surface (QP), Fig. S3 shows that there was no significant variation in colour parameters with firing times. The values of L* ranged from 45 to 52, a* ranged from 27 to 30, and b* ranged from 44 to 51 when heated at 900 °C (Table S1 and Fig. S4). Temperature seemed to have a darkening effect above 1000 °C (Fig. S3 and Table S1). Up to 900 °C, the L* coordinate remained constant, between 47 and 52, and above 900°, it progressively decreased to 34 (1100 °C) (Table S1 and Fig. S4). Visually, this darkening became more evident between 1000 and 1100 °C (Fig. S3). The a* and b* coordinates did not show significant variation with time and temperature, remaining in the ranges of 27–30 and 42–50, respectively (Table S1 and Fig. S4). The dispersion of the colorimetric results of the archaeological samples was greater than that of the QP samples (L* = 44–61; a* = 13–28; b* = 23–49), so it was not possible to establish close values of temperatures or time ranges (Table S1 and Fig. S4).

The samples used to simulate the inside of the tile body (CU) showed a greater dependence on firing times and temperatures. At 900 °C and for firing times of <24 h, a greyish area appeared inside the samples (Fig. S3). The radius of this grey zone was progressively reduced with increasing temperature until it disappeared after 24 h of firing (Fig. S3). The coordinates that varied the most were a* and b*, with low values ranging from 5 to 8 and 7–12 (greyish hues) for times of 1, 3 and 6 h, which increased until values similar to those of the QP samples (30–32 and 49–55) were reached for times of 24, 48 and 72 h. The L* coordinate decreased from 52 at 1 h to 44 at 72 h (Table S1 and Fig. S4).

Regarding colour variations with temperature with firing for 24 h, the CU samples fired at 700 °C were a lighter colour (L* = 52, a* = 18, and b* = 36) than those fired at 800–900 °C (L* = 47–46, a* = 29–30, and b* = 44–49) and the QP samples (Table S1 and Fig. S4). The darkening process in high-temperature samples started at 950 °C (L* = 42, a* = 27, and b* = 41), instead of 1000 °C, as occurred in the QP samples (Table S1 and Fig. S4). The colour in the CU samples (L* = 25, a* = 22, and b* = 35) reached at 1100 °C was a darker red than the QP samples (L* = 34, a* = 28, and b* = 43) under the same experimental conditions (Fig. S3, Table S1 and Fig. S4).

A firing time >24 h could be established due to the absence of dark regions inside most of the archaeological samples found in Tiebas (Ruiz-Ardanaz et al., 2021). Above 24 h, no upper limit of the time range and no temperature range could be set. Additional techniques were needed to determine a narrower range of temperatures and times, as seen below.

3.2. Fourier transform infrared (FTIR) spectroscopy

Infrared spectroscopy analysis of the archaeological samples showed the samples to be mainly quartz and other minor silicates as well as secondary (recarbonated) calcite, but only in a few samples (Ruiz-Ardanaz et al., 2021; Jordanova et al., 2019). The *replica* samples (Figs. S5 and S6) exhibited the same signs of quartz and silicates that appeared in the archaeological tile bodies (i.e., tile M9): a Si—O bending band at 695 cm^{-1} (**δ** Si—O), Si—O *sym*metric stretching bands at 780 and 795 cm^{-1} (sym **ν** Si—O), a broad Si—O *asym*metric stretching band between 950 and 1080 cm^{-1} (asym **ν** Si—O), and a small band in the shoulder of the Si—O asymmetric stretching band at 1160 cm^{-1} (asym **ν** Si—O) (De Benedetto et al., 2002; MDHS101, 2005; Legodi and de Waal, 2007; Nodari et al., 2007; Medeghini et al., 2016; Daghmehchi et al., 2018; Măruţoiu et al., 2018). The spectrum of raw clay (A15) was also depicted for comparative purposes. In raw clay (A15), Si—O asymmetric stretching signals in the range of 950–1050 cm^{-1} shifted at minor wavenumber values compared to those of the fired samples (archaeological and *replica*) (Figs. S5 and S6). The Si—O asymmetric stretching band (asym **ν** Si—O) of illite was seen at 905 cm^{-1} (Daghmehchi et al., 2018). Other absorption bands of illite appeared at ca. 752 and 3610 cm^{-1} for raw clay and were slightly detected in the QP samples fired at 700 °C for 24 h (Legodi and de Waal, 2007).

Regarding the differences between the *replica* samples (QP and CU), different bands were observed, but only a change in the absorbance intensity of the three Si—O asymmetric stretching bands was observed: 950–1050, 1060 and 1080 cm^{-1}. For the samples fired for 24 h, the changes in the intensity of the broad band between 950 and 1080 cm^{-1} towards higher wavenumbers were observed to be proportional to the firing temperature for both QP and CU (Figs. S5a and S6a). The ratio of the signals at 1080 and 1060 cm^{-1} (both assigned to the Si—O asymmetric stretching band) increased for the sampled fired at the highest temperature, 1100 °C (Figs. S5a and S6a). The displacement and the increase in the ratio are related to the ordering changes of the silicon and oxygen atoms of the quartz that occur during sintering and glass formation (Legodi and de Waal, 2007; Medeghini et al., 2016). Incipient transformation of the two symmetric strain bands of quartz at 780 and 795 cm^{-1} (sym **ν** Si—O) into one peak is characteristic of cristobalite (SiO_2) (MDHS101, 2005) and was also observed in Figs. S5 and S6 for firing temperatures above 1000 °C. No notable changes were observed with firing time, which means that it barely affects mineral changes (Figs. S5b and S6b). The comparison of the results of the cubic samples (CU) and the quadrangular prisms (QP) indicate that the shift towards higher wavenumbers occurs on the surface rather than inside, suggesting greater sintering and/or melting and glass formation on the surface.

Comparison of the *replica* and the archaeological sample spectra allows us to estimate a range of firing temperatures between 800 and 1000 °C. However, the FTIR study did not allow us to distinguish between firing times.

3.3. X-ray diffraction (XRD)

The characterisation of the archaeological samples by XRD showed that the composition was primarily quartz, with some minor phases,

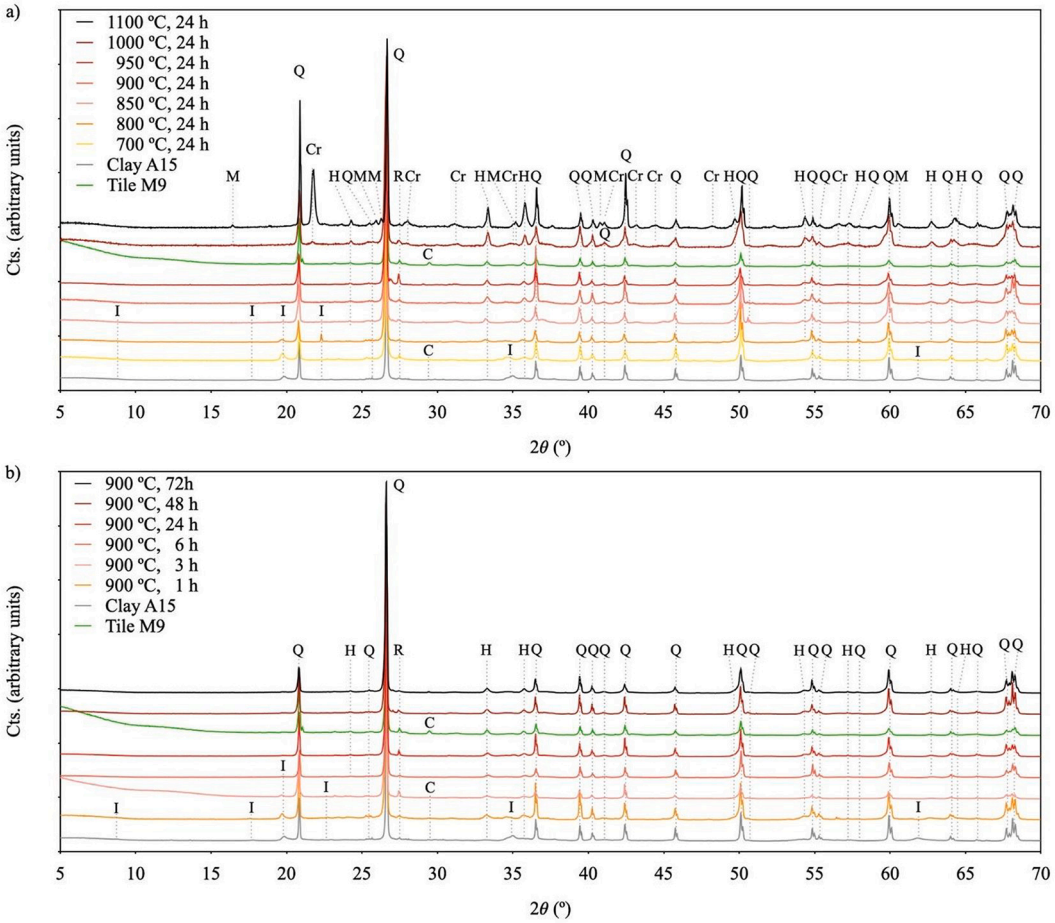

Fig. 3. X-ray diffraction patterns of experimental *replica* QP samples fired for 24 h at different firing temperatures (a) and at 900 °C for different firing times (b). The patterns of an archaeological sample (M9) and the raw clay (clay A15) are also depicted. Abbreviations: Q–quartz (file 33–1161); R–rutile (file 21–1276); I–illite (file 70–3754); H–haematite (file 33–0664); C–calcite (file 05–0586); Cr–cristobalite (file 39–1425); and M–mullite (file 15–0776).

such as haematite, micas (illite) and potassium feldspar (orthoclase, $KAlSi_3O_8$) (Ruiz-Ardanaz et al., 2021). In some samples, some very minor calcite phases were also detected (Ruiz-Ardanaz et al., 2021).

In the *replica* samples, quartz was predominant, and no variations in this phase with firing temperature or firing time were observed (Figs. 3 and 4). In contrast, the presence and relative amounts of other phases were related to time (hercynite ($Fe^{2+}Al_2O_4$) and illite) or firing temperatures (illite, calcite, haematite, mullite ($Al_6Si_2O_{13}$) and cristobalite).

In order to identify the characteristic minerals depending on heating temperatures and times, PCA were carried out in all the diffractograms of the *replica* samples (CU and QP).

In all the PCAs the two main components showed a sum of 81–97% in variability. The results of the matrix of scores (U) did not show a proportionality with the firing conditions of the *replicas* (Fig. S7), so they could not be used as variables to determine the original heating conditions. However, the analysis of the coefficients of these two main components made possible to identify the reflections (Bragg angles) with the greatest variability, and therefore, they were considered as interesting angles. Table 3 showed the reflections that have been identified in the coefficients of the two main components of each set of *replicas*. The most relevant were the reflections of quartz and haematite as they were the most frequent in all the sets. Some reflections of illite ($2\theta = 19.7, 22.3, 35.2, 61.9$), calcite ($2\theta = 29.5$), rutile ($2\theta = 27.4$) and cristobalite ($2\theta = 21.7$) also appeared as relevant, although they were less frequent or did not appeared in all sets of *replicas*. Although quartz reflections identified by PCA were very frequent, no proportionalities with firing conditions were found. This could be due to the fact that being such an abundant mineral, any minimal error in the Bragg angle values or in the relative intensity of their reflections generated variability. This variability was detected by PCA but was not necessarily related to firing conditions. On the contrary, the haematite reflections identified by PCA were related to the firing conditions, their intensity being directly proportional to them, as will be seen below. According to the analysis of the PCA coefficients (Table 3), reflections $2\theta = 33.3$ (104) and $2\theta = 35.7$ (110) were of special relevance.

Within the mineral phases dependent on the firing time, hercynite was found, which only appeared inside the cubic samples (CU) and at firing times <24 h (Fig. 4b and Table S2). The presence of hercynite was probably the cause of the dark colour seen inside the cubic samples (values of a* and b* were <8 and 12, respectively, for heating times up to 6 h, Fig. S3a, Table S1 and Fig. S4). However, as time increased, the volume of this dark area decreased until it disappeared after 24 h of firing. The values of a* and b* were higher than 30 and 49, respectively, after 24 h of heating. The presence of phases containing Fe(II), such as hercynite, was related to reducing atmospheres (high CO) that reduce the Fe(III) present in different minerals (Maritan et al., 2020). However, hercynite phases have also been identified in samples heated in neutral atmospheres at high temperature (Jordán et al., 1999; Noghani and Emami, 2014; Maritan et al., 2020). This last case seems to match the results obtained in this study, since the darkened area only corresponds to the inside of the samples, where the ambient oxygen took time to reach. This effect was not seen in the QP samples because they were much thinner, as was the case in the most superficial part of the CU samples. All of these explain why for long firing times, hercynite was

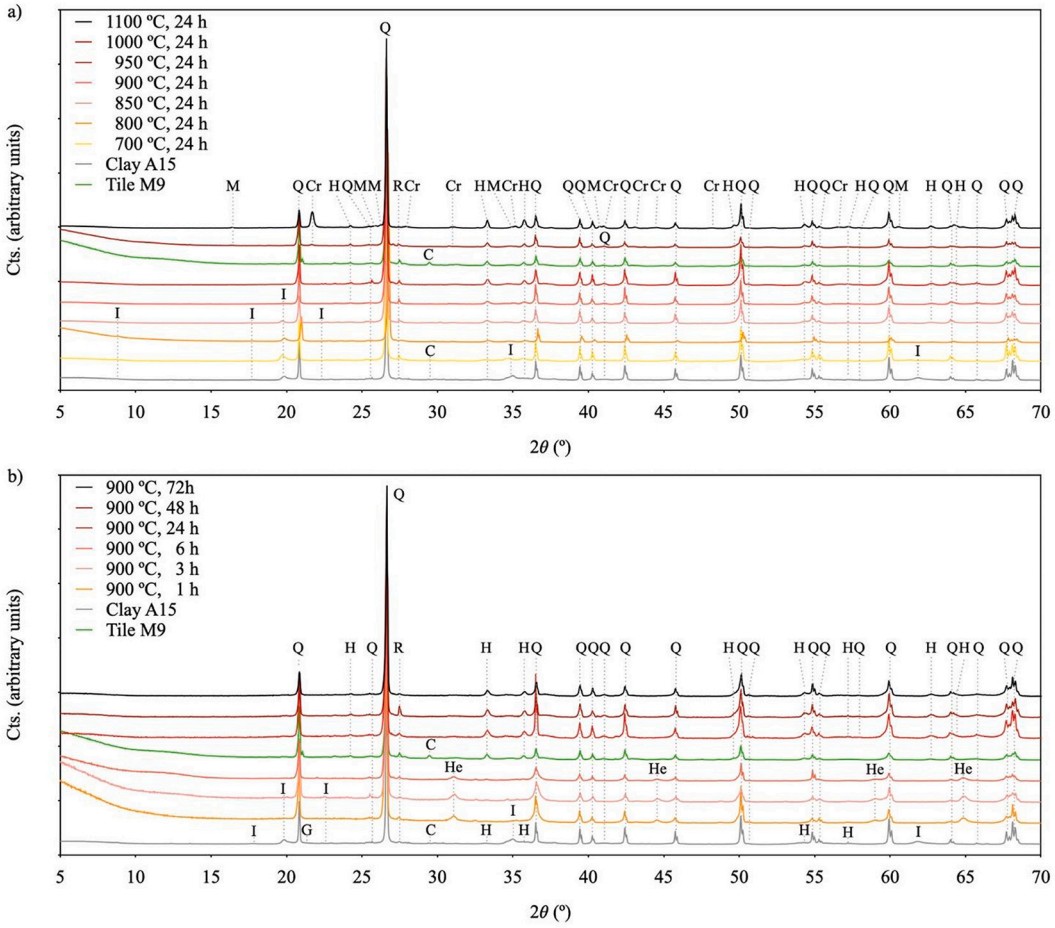

Fig. 4. X-ray diffraction patterns of experimental *replica* CU samples fired for 24 h at different firing temperatures (a) and at 900 °C for different firing times (b). The patterns of an archaeological sample (M9) and the raw clay (clay A15) are also depicted. Abbreviations: Q–quartz (file 33–1161); R–rutile (file 21–1276); I–illite (file 70–3754); H–haematite (file 33–0664); C–calcite (file 05–0586); He–hercynite (file 34–0192); Cr–cristobalite (file 39–1425); and M–mullite (file 15–0776).

Table 3
Results of the analysis of the matrix of coefficients of the main components grouped by the analysed *replica* sets. For each replica set the % of variance explained by the principal (C_1) and secondary (C_2) components. Reflections identified by the PCA as significant are shown. Abbreviations: Q–quartz (file 33–1161); R–rutile (file 21–1276); I–illite (file 70–3754); H–haematite (file 33–0664); C–calcite (file 05–0586); Cr–cristobalite (file 39–1425).

QP *replicas*, $t = 24$ h $C_1 = 71.5\%$; $C_2 = 17.6\%$		QP *replicas*, $T = 900$ °C $C_1 = 44.8\%$; $C_2 = 42.0\%$		CU *replicas*, t = 24 h $C_1 = 63.8\%$; $C_2 = 17.2\%$		CU *replicas*, T = 900 °C $C_1 = 60.7\%$; $C_2 = 36.3\%$	
Reflection (2θ)	Mineral phase	Reflection (2θ)	Mineral phase	Reflection (2θ)	Mineral phase	Reflection (2θ)	Mineral phase
19.7	I (020)	19.7	I (110)	19.7	I (110)	20.8	Q (100)
20.8	Q (100)	21.0	Q (100)	20.8	Q (100)	24.2	H (012)
21.7	Cr (101)	33.3	H (104)	21.8	Cr (101)	27.4	R (110)
24.2	H (012)	35.8	H (110)	22.3	I	33.4	H (104)
26.6	Q (101)	40.3	Q (012)	26.6	Q (101)	35.2	I
27.4	R (110)	42.6	Q (200)	27.5	R (110)	35.7	H (110)
29.5	C (104)	45.6	Q (201)	33.0	H (104)	36.5	Q (110)
33.3	H (104)	49.7	H (024)	35.6	H (110)	50.2	Q (112)
35.7	H (110)	54.3	H (116)	36.5	Q (110)		
36.5	Q (110)	62.8	H (018)	39.4	Q (102)		
39.3	Q (102)			45.8	Q (021)		
42.4	Q (200)			50.1	Q (112)		
49.8	H (024)			54.8	Q (202)		
				55.6	Q (103)		
				57.9	Q		
				61. 9	I		

replaced by haematite, even inside the cubic samples (Fig. 4). Haematite was detected after 24 h of heating (Fig. 4a), very possibly due to the oxidation of iron to Fe(III). The black core of the *replica* samples gradually faded with increasing time and firing temperature (De Bonis et al., 2017).

The absence of hercynite in the archaeological samples was an excellent indicator of a firing time equal to or >24 h.

Illite only appeared at low firing temperatures and short times and progressively disappeared when both increased. Fig. S8 represents how the relative abundance of illite evolved with firing times and temperatures, expressed as the count intensity ratio of the maximum reflection at $2\theta = 19.8°$ ((020) reflection of illite, PDF 70–2754) and the maximum reflection at $2\theta = 26.6°$ ((101) reflection of quartz, PDF 33–1161). The temperature at which it disappeared depended on the firing time and vice versa (Fig. S8 and Table S2). In QP samples fired for long times (24–72 h), the temperature at which illite disappeared was 850 °C, while with short firing times (1−3h), it disappeared at 950 °C (Fig. S8). In the case of the CU samples, illite completely disappeared at 950 °C and 24 h. Thus, it was deduced that the thickness of the sample affected the minimum firing times and temperatures for illite elimination, retarding both. The abundance of illite in the archaeological tiles from Tiebas was very low but detectable in most. In Fig. S8, the abundances found in the archaeological tiles were marked with a diffuse yellow stripe, very close to the nonsignificant detection level (<1%). From these results, a range of firing times longer than 6 h and temperatures higher than 800–850 °C were deduced.

In general, mullite and cristobalite are phases that only appear in the archaeological samples when they are heated at very high temperatures (1000–1100 °C). The first originates from the combination of decomposed illite and amorphous SiO_2, while the second originates directly from amorphous SiO_2 and quartz (Chen et al., 2000; Traoré et al., 2003; Aras, 2004; Martín-Márquez et al., 2008; Baccour et al., 2009; Pérez-Monserrat et al., 2019). In the *replica* samples, both phases began to appear at 1000 °C, and at 1100 °C, they became much more evident. The relative abundance of both phases increased with increasing firing times for CU samples. The absence of mullite and cristobalite in the archaeological samples from Tiebas reduced the upper limit of the temperature range at 950 °C, the highest at which they were not detected in the experimental samples (Table S2).

Haematite, unlike the previous phases, did not appear or disappear but was present in all cases (Figs. 3, 4 and Tables S2 and S3), except when transformation into hercynite occurred. However, the intensity of this phase was proportional to the heating temperatures, so it could be used to more precisely determine the firing temperatures of the archaeological samples by extrapolating the results found for the experimental samples (Fig. 5a,c). Similar to Fig. S8, Fig. 5a,c represents the relative abundance of haematite depending on firing times and temperatures, expressed as the count intensity ratio of the maximum reflection at $2\theta = 33.3°$ ((104) reflection of haematite, PDF 33–0664) and the maximum reflection at $2\theta = 26.6°$ ((101) reflection of quartz, PDF 33–1161). The reddish colour of ceramics is closely related to their haematite content, which is the main cause of the red colour in this type of material (Torrent et al., 1983; Torrent and Barrón, 2003; Backes et al., 2012). The decreasing CIEL*a*b* coordinates of *replica* samples (Fig. S3, Table S1) with increasing temperatures were related to the relative abundance of haematite (Fig. 5a,c). The darkening of *replica* samples that occurred between 1000 and 1100 °C matched the increase in haematite relative abundance at the same firing temperatures. The haematite/dark red colour relationship also explained the greater darkening of the CU samples at 1000 and 1100 °C with respect to the QP samples (Fig. S3, Table S1).

Furthermore, the haematite reflection width (considering the signal at $2\theta = 33.3°$) is inversely proportional to firing temperature and can be used to determine crystal sizes using Scherrer's equation (Fig. 5b-d). The colour of the *replica* samples (Fig. S3, Tables S1 and S3) was related to the haematite crystal size, as is its relative abundance. The firing time and temperature evolution of the haematite crystal size is described as sigmoidal. The growth in the crystal size values remained constant between 700 and 850 °C, increased rapidly between 850 and 950 °C, and increased more slowly above 950 °C (Fig. 5 and Table S3).

Regarding the evolution depending on firing times during the first 6 h, the crystal sizes increased rapidly, while after 6 h, the growth in crystal size was much slower (Fig. 5b,d and Table S3). The CU samples showed an increase in crystal size with respect to the QP samples under the same firing conditions. The comparison of the relative abundance and crystal sizes of the haematite in the archaeological samples and the experimental samples indicated a firing temperature between 925 and 1050 °C and an indeterminate firing time. Fig. 5d shows how temperature and precise times were related and how one cannot be determined without the other.

3.4. Acid digestion resistance (Colour and XRF)

Another factor closely related to the firing conditions is the sintering process and the porosity changes of the ceramics (Tite, 1969; Martín-Márquez et al., 2008; Pérez-Monserrat et al., 2019). When the firing

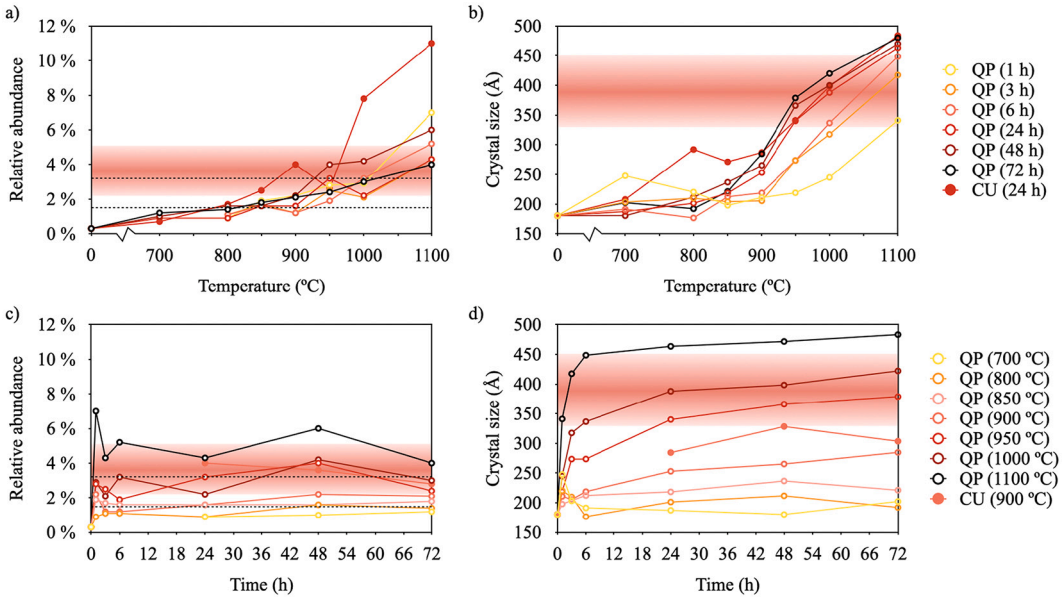

Fig. 5. (a,c) Relative abundance and (b,d) crystal size of haematite ($2\theta = 33.3°$) depending on (a,b) firing temperatures and (c,d) firing times, sorted by experimental sample type and firing conditions. The relative abundance range and crystal size range of the archaeological tiles are indicated by fuzzy red horizontal lines. (a,c) The limit of detection (LOD) and quantification (LOQ) are represented by black dashed lines.

temperature increases, the mineral reactions and the surface fusion of silicate crystals favour sintering (Tite, 1969; Martín-Márquez et al., 2008; Pérez-Monserrat et al., 2019). In the IR spectra of *replica* samples, the sintering processes increased at the highest temperatures, mainly in the QP samples (Figs. S5 and S6). This implies a reduction in the ceramic porosity and the differential possibility of the dissolution and/or attack of the minerals within (Tite, 1969; Martín-Márquez et al., 2008; Pérez-Monserrat et al., 2019). Because haematite is soluble in *aqua regia*, while quartz and some silicates are not, the attack of haematite under different firing conditions was studied. After an attack combining acidic media (*aqua regia*) and microwave treatment of the *replica* and archaeological samples, the resulting solid residue was analysed.

In Fig. 6, the colour changes of the undigested residue corresponding to the same samples depicted in Fig. S3 can be seen. Colour coordinates of the sample residues shown in Fig. 6 are presented in Table S1 and Fig. 7. The undigested residues showed (Fig. 6) a greater colour change than the undigested powder samples (Fig. S3). For QP samples after acid treatment, L* drastically decreased with increasing firing temperature,

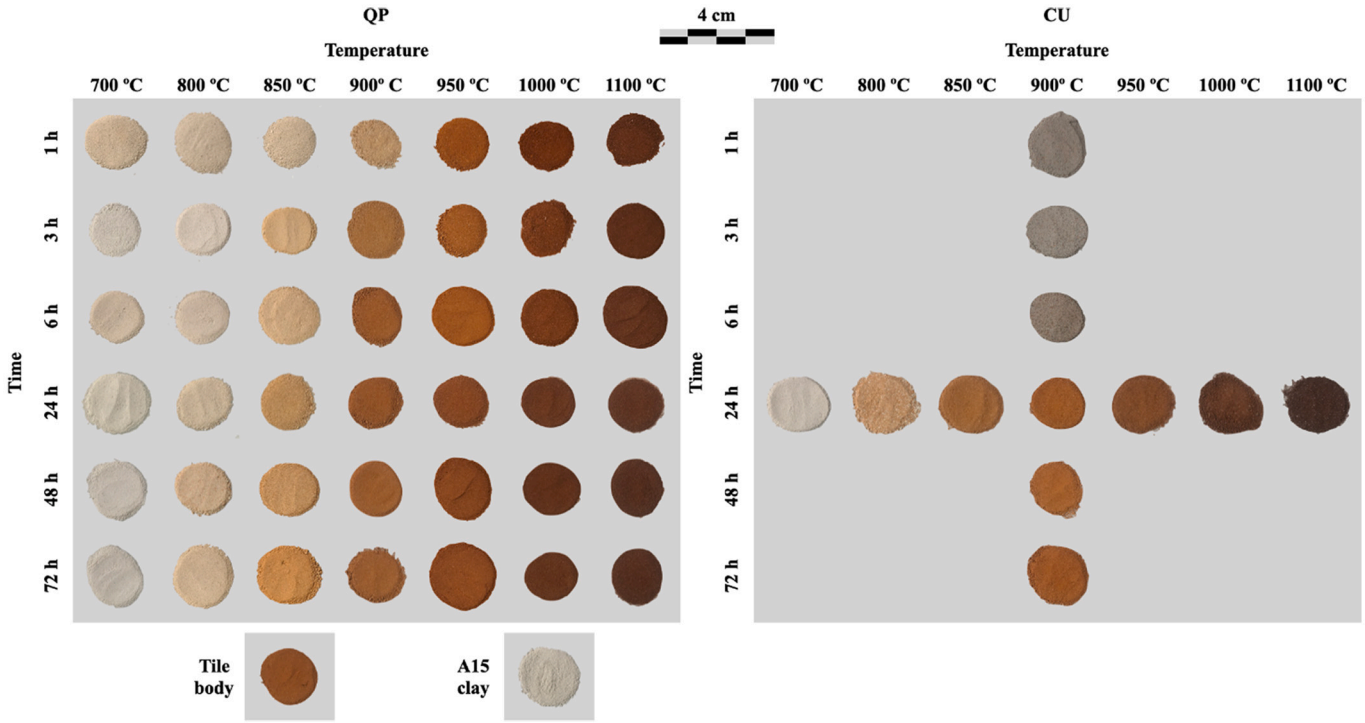

Fig. 6. Images of the *replica* sample residues after acid digestion, sorted by sample type, firing temperature and firing time. Images of the archaeological tile residue (M4) and the clay (A15) after acid digestion are shown at the bottom left.

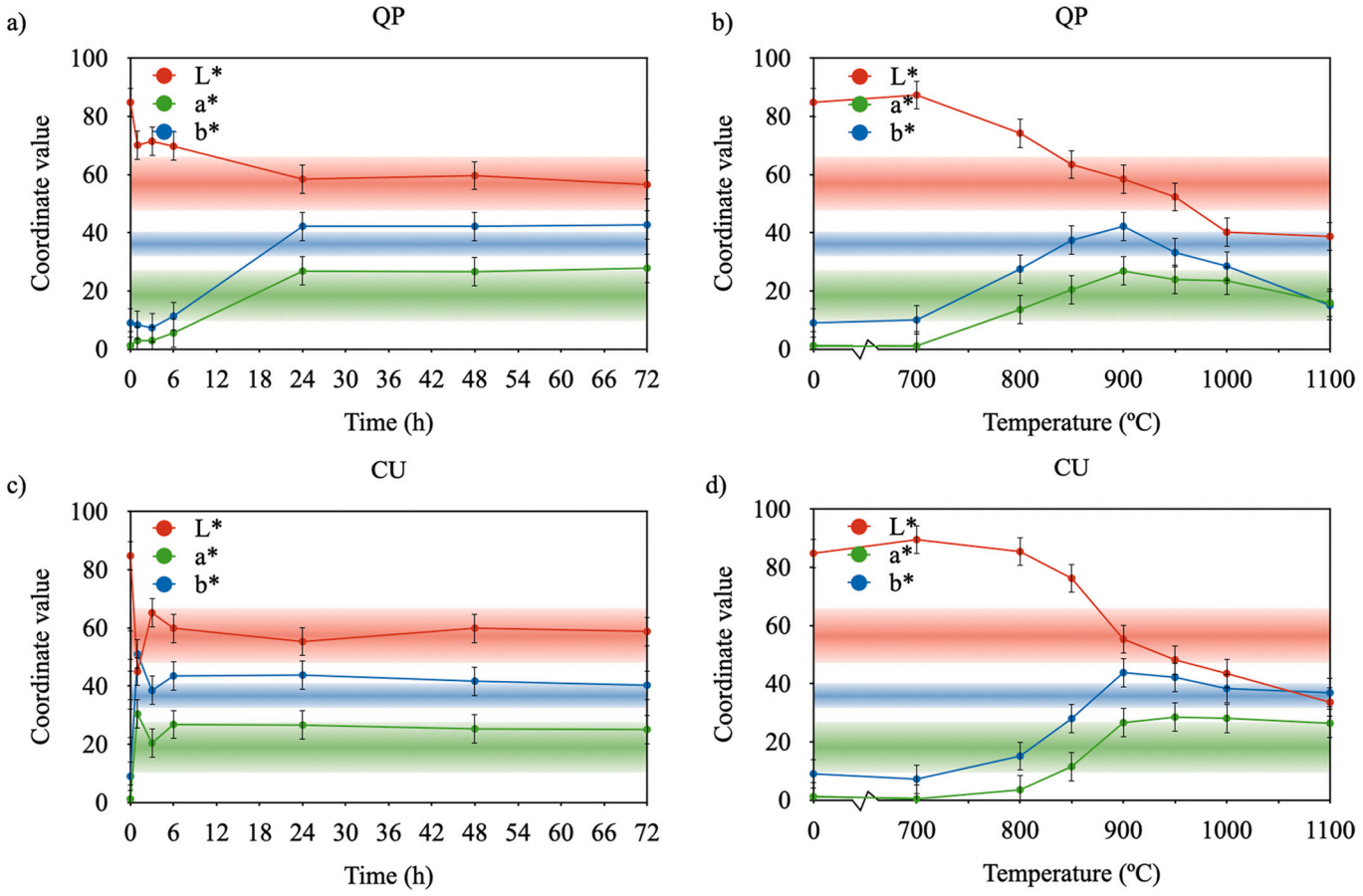

Fig. 7. Evolution of the CIEL*a*b* coordinates of the digestion residues of *replica* samples with firing time at 900 °C (a,c) and firing temperature for 24 h (b,d). The colour range of the archaeological tiles is indicated by fuzzy horizontal lines for each coordinate.

and the a* and b* coordinates increased in almost all cases below 900 °C and then decreased until 1100 °C was reached (Table S1 and Fig. 7). For the CU samples, at 900 °C, the values of L* decreased but did not decrease as drastically as in the QP samples, and a* and b* increased with increasing firing time (Table S1 and Fig. 7). At 24 h of firing, the values of a* and b* increased until 900 °C was reached and then

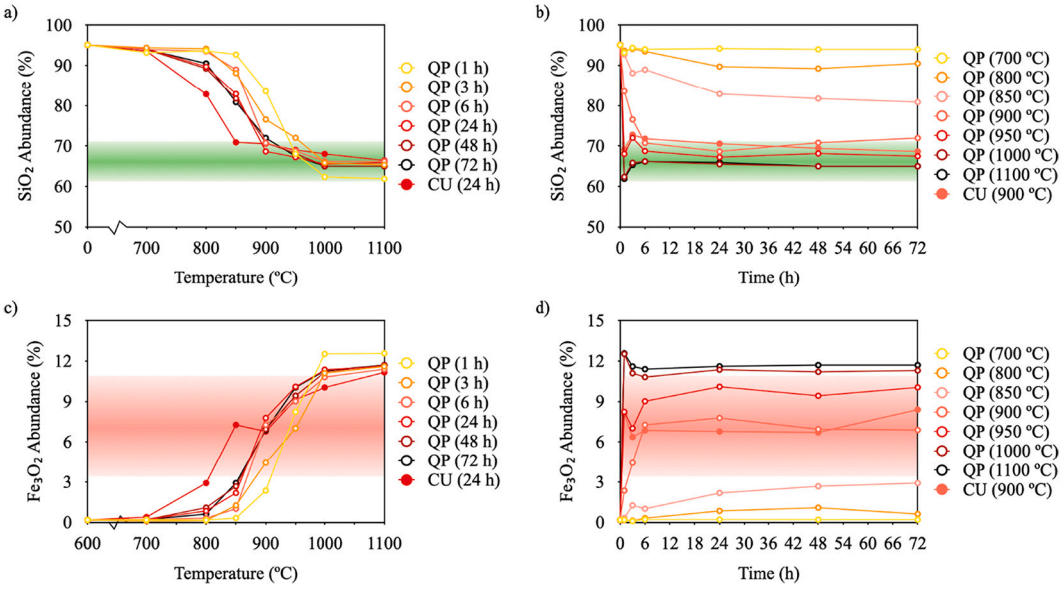

Fig. 8. Abundance of Si and Fe oxides with (a,c) firing temperature and (b,d) firing time, sorted by experimental sample type and firing conditions. The relative abundance range and crystal size range of the archaeological tiles are indicated by fuzzy red horizontal lines. (For interpretation of the references to colour in this figure legend, the reader is referred to the web version of this article.)

decreased, similar to those of the QP samples. Visually, the CU samples retained the dark grey colour related to hercynite, so there were no differences between the iron mineral phases (haematite or hercynite) in terms of the accessibility of sintered ceramics attacked with *aqua regia*. The CU samples presented a darker colour than the QP samples under the same firing conditions, which means a greater change with decreasing firing time and temperature.

Regarding the mineralogical phases found in the undigested residues, neither haematite nor hercynite was detected in the samples heated for the shortest times (1 h) at the lowest temperatures (700 °C) (Fig. S9). When increasing both factors, the extent of sintering increased, allowing the detection of haematite in QP samples fired for >24 h at >850 °C and hercynite or haematite in all *replica* samples fired above 800 °C (Fig. S9). This is related to the protective role played by silicate phases in sintering in preventing iron compounds from being attacked. The colour of the archaeological sample residues was similar to that of experimental samples fired at 900–1000 °C. Regarding firing times, the absence of hercynite and the dark colour seen in the inner part of the archaeological samples indicated a firing time longer than 24 h.

Fig. 8 shows how the relative abundance of SiO_2 and Fe_2O_3 in the samples evolves with time and temperature variations. At low temperatures and short times, quartz was the major phase in proportion due to the loss by the dissolution of some other compounds based on Fe, K, Mg, and Ca. The white colour (high L* value and low a* and b* values) of sample residues fired at short times and low temperatures was related to the quartz abundance and the absence of haematite (Table S1 and Fig. S9). At high firing temperatures and long times, the opposite effect occurred (lower L* values and high a* and b* values), showing the high relative amounts of Fe_2O_3, the sintering of the material and the reduction in the internal porosity, so protecting iron-based compounds against acid attack (Tite, 1969; Martín-Márquez et al., 2008; Pérez-Monserrat et al., 2019). Sintering basically involves of the formation of glass zones between mineral crystals, in this case, quartz crystals (Tite, 1969; Martín-Márquez et al., 2008; Pérez-Monserrat et al., 2019). The red colour of these other samples was related to their higher haematite content (Table S1 and Fig. S9). The CU samples showed a lower sintering temperature than the QP samples (50 °C lower). As in the case of residue colour, the abundance of silicon and iron oxide indicated a firing temperature range of 850–1000 °C. The firing time range could not be estimated. Therefore, the elemental composition of the sample residues seems to be a valuable variable to model to determine the firing conditions of the archaeological samples. Alternative methods were explored in order to evaluate the porosity of the ceramics, such as that employing the IR spectra (De Los Arcos et al., 2021) but the results found were not satisfactory.

3.5. Firing temperature and time models

As mentioned above, firing temperatures and times were closely related, and both influenced the physicochemical properties of the samples. Increases in temperatures reduced the firing times and vice versa. That is why it was mandatory to analyse both variables together as a three-variable system. The system was composed of an analytical variable measured with a physicochemical technique and the methodological variables, firing temperatures and times. Ideally, the analytical variable is linearly proportional to time and temperature so that an experimental equation describing the system can be obtained through a regression relationship. The original firing conditions of the archaeological samples were obtained by extrapolating the analytical values from *replica* samples in the equation obtained thanks to a model. However, in our case, the analytical variables obtained did not follow a linear function with temperature and time (Figs. S8, 5, 8). The analytical variables obtained followed a sigmoid function, which could be linearized by different equations (Zullinger et al., 1984; Majer, 1995; Xiong et al., 1999; Yin et al., 2003).

As analytical variables, those with the greatest variation ranges and the best proportionality were selected: haematite crystal size in undigested samples (HCS, Fig. 5b-d, Table S3) and some relevant major element oxides in digestion residues (% SiO_2 and % Fe_2O_3) (Fig. 8, Tables S4 and S8). The results used for modelling were only those of the QP samples since they covered all times and temperatures. The results of the CU samples were later superimposed on the model to assess their differences.

Of all the sigmoid equations tested (logistic eq., Gompertz eq., and Cole eq.), the one that best describes the three-dimensional systems of temperature, time and each analytic variable (HCS, %SiO_2, and %Fe_2O_3) was the following (Zullinger et al., 1984; Majer, 1995):

$$\text{Variable} = A + \frac{B}{1 + 0.5\, e^{-\alpha}} \tag{2}$$

In Eq. (2), A and B are constants. A corresponds to the minimum value of the analytical variable, and B corresponds to the difference between the minimum and maximum values of the analytical variable. Because the behaviour of the haematite crystal size (HCS) followed a different sigmoidal function than that describing the elemental composition of % SiO_2 and % Fe_2O_3, two variants of the model were used: variant one for the variable HCS and variant two for the variables % SiO_2 and % Fe_2O_3. Alpha was a pseudo variable that depended on time and temperature. Although Eq. (2) was the same for both variants, the alpha exponent was different in each analytical variable and was substituted in Eq. (2) as $\boldsymbol{\alpha}_1$ (for HCS, as all the subindexes of variable 1) or $\boldsymbol{\alpha}_2$ (for % SiO_2 and % Fe_2O_3, as all the subindexes of variable 2):

$$\alpha_1 = \frac{T - C/t - D}{E/t + F} \tag{3}$$

$$\alpha_2 = C\,T\,ln(t) + D\,T - E\,ln(t) - F \tag{4}$$

Three linear regressions were used to model the analytical results. The first regression adjusted the analytical data with firing temperatures, keeping firing time constant. The second and third regressions optimised the coefficients of the first regression considering firing times. In Eqs. (3) and (4), C, D, E and F are the coefficients obtained from three linear regressions applied to each. For these linear regressions of both variants of alpha, the analytic variable was transformed with the following formula to obtain the pseudo variable $\boldsymbol{\alpha}$ from Eq. (2):

$$ln(1/2) - ln\left(\frac{B}{Variable - A} - 1\right) = \alpha \tag{5}$$

From Eq. (5), the first linear regression was performed by substituting it into the following equations:

$$\alpha_1 = \frac{T - C'_1}{E'_1} \tag{6}$$

$$\alpha_2 = C'_1\,T - E'_2 \tag{7}$$

The first regression was performed for each series of temperatures (T) and analytical data (HCS, %SiO_2, and %Fe_2O_3) with the same firing time (Figs. S10, S11 and S12). C' and E' are pseudo constants that were obtained from the slope and y-intercept of the linear regression, respectively. Eqs. (6) and (7) are analogous to Eqs. (3) and (4) except that the firing times and other constants are included within the pseudo constants C' and E'. Once the pseudo constants C′ and E' were obtained for each time, the remaining constants were determined by a linear regression:

$$C'_1 = C/t + D \tag{8}$$

$$E'_1 = E/t + F \tag{9}$$

$$C'_2 = C\,ln(t) + D \tag{10}$$

$$E'_2 = E\,ln(t) + F \tag{11}$$

Regressions were performed for each series of pseudo constants and firing times (Figs. S10, S11 and S12). *C* and *E* were obtained from the slope of the linear regression, since *D* and *F* were obtained from the y-intercept (Figs. S10, S11 and S12). Table 4 shows the model constants that were obtained from the three regressions of each experimental variable.

Once the constants of both variants (1 and 2) of the sigmoid model were defined, the values of the analytical variables could be predicted for any time or temperature (Fig. 9). The model used for haematite crystal size (HCS) shows how the sizes increased with time in the first few hours and then remained constant. The variations with temperatur were much slower and progressive, and only a large increase from 800 °C to 1100 °C took place. The behaviour of the experimental data (Fig. 9a) was very similar to that of the built model (Figs. S10, S11 and S12). In the case of the percentages of SiO_2 and Fe_2O_3, at low firing temperatures and times, most of the soluble components were lost (low $\%Fe_2O_3$), so the SiO_2 content was very high. In contrast, by increasing the times and temperatures, the sintering process increased, and porosity decreased; thus, the soluble elements were better retained, and higher $\%Fe_2O_3$ and minor SiO_2 contents were detected. In this last case, despite being attacked with *aqua regia*, the amounts of % SiO_2 and % Fe_2O_3 were almost the same as those detected without attack, approaching the value of the nondigested samples (63% SiO_2, 12% Fe_2O_3).

The goodness of fit of each regression was evaluated using the coefficient of determination (Table 5). The coefficient of determination was >0.95 in most cases. However, the coefficients of determination in some regressions are lower (but higher than 0.83), although they are the best of all the sigmoid functions that have been tested to describe the models.

To check the precision of the model, the differences between the experimental data and the corresponding data in the model were evaluated. The difference between the experimental data and their respective data from the model was normalised with the constant B, since it represents the maximum variation of each model and allows for the comparison of variables (HCS, $\%SiO_2$, and $\%Fe_2O_3$). In addition, the same differences were calculated with the intermediate model obtained from the first regression (which kept firing time constant and only considered the effect of firing temperature). From the results in Table 5, the first regression provided the smallest difference between the experimental data and those obtained from the models (Δ%Var in Table 5). In the case of HCS, the second and third regressions (with constant firing time and only considering the effect of firing temperature) increased the total difference (−1.7% ± 6.1%) more than the first regression (−1.7% ± 5.3%). This means that the fit with firing times was better than the fit with firing temperatures. However, in all cases, the differences between the model and experimental data were <10% (value of ± STD).

The main advantage of these three-dimensional models is that they simultaneously considered the variables firing time and firing temperature. In this way, it was possible to obtain, by extrapolating the analytical results of the archaeological samples, the theoretical conditions that were used in their manufacture in the 13th century. The results obtained for the archaeological samples were haematite crystal sizes of 390 ± 60 Å and digestion residue compositions of 66 ± 4% SiO_2 and 8 ± 3% Fe_2O_3. The graphs in Fig. 10 were obtained by substituting these results in their respective empirical equations from the model.

For the three experimental factors (HCS, % SiO_2 and % Fe_2O_3) obtained for the QP samples (Fig. 10a, b and c, respectively), similar firing temperatures were observed, varying in the range between 925 and 1000 °C. The firing time was unimportant for times longer than 12 h (Fig. 10). However, for times <12 h, time was clearly a variable to assess.

The superposition of the experimental results obtained for the CU samples from the built model (from QP samples) indicated some differences compared with those obtained for the QP samples. The depicted values were above the HCS and % Fe_2O_3 models and below the % SiO_2 model. From these results, it was estimated that the firing temperature inside the tiles was approximately 50 °C lower than that of its surface. The range of temperature values for archaeological samples was estimated to be between 875 and 950 °C. No differences were detected in firing time between the experimental results of the CU samples and the model obtained from the QP samples.

As mentioned above, the available literature on *carreaux de pavement* briefly mentions some approximate firing time and temperature values. The data provided (Table 6) are generally based on other literature references (concerning glaze melting) rather than on experimental determinations. The detection of gehlenite is the only reference for experimental detection (Ben Amara et al., 2005). Gehlenite was not detected in our studied experimental *replica* and archaeological samples, so it could not be used as a marker of firing temperature.

The firing time and temperature values provided in the literature for the *carreaux de pavement* (800–1000 °C), despite not being based on experimental data, are similar to those obtained experimentally in this article (875 and 950 °C). However, the temperature range provided by this new publication is much narrower and more precise.

Regarding the firing time, only one reference was found (Table 6), and it referred to a firing time of two days, including an initial heating time of a few hours and a low temperature to remove moisture (Norton, 1992). Firing for almost two days is compatible with the results obtained experimentally in the replicas (>24 h).

3.6. Compressive strength

Several investigations have found a direct relation between firing time and temperature and physical and mechanical properties (Tite et al., 2003; Cultrone et al., 2004; Karaman et al., 2006; Moses and Ben, 2018). The mineral composition of the pastes or their resistance to acid was unknown in the 13th century. Conversely, the compressive strength was one of the physical properties that mattered to mediaeval craftsmen. Thus, compressive strength is one of the most crucial characteristics to assess. Mechanical property tests usually require the destruction of a large volume of archaeological samples. In this paper, the study of *replica* samples under the same manufacturing conditions as the original archaeological samples allowed for the determination of their mechanical properties without the need to damage the archaeological samples.

For the compressive strength tests, the CU samples were used since they had a thickness similar to that of the archaeological samples. The cubic samples (CU) were tested in triplicate, showing a progressive increase in values with increasing firing time (Fig. S13a). The behaviour was more irregular with temperature (Fig. S13b).

Considering the firing conditions deduced in the previous sections, a compressive strength between 50 and 80 MPa could be estimated (Fig. S13). The range of firing temperatures and times coincided with the highest strength achieved in the experimental samples, so the firing conditions used by these mediaeval craftsmen were optimal for

Table 4
Optimised constants of the acquired experimental models for Eq. (2) with their two variants (Eqs. (3) and (4)).

Variable	A (%)	B (%)	C1 (°C·h)	D1 (°C)	E1 (°C·h)	F1 (°C)	C2 (°C)	D2 (°C)	E2	F2
HCS	176.6	307.2	251.6	977.2	60.8	53.4	–	–	–	–
SiO_2	94.4	−33.3	–	–	–	–	−5	0.04	−4.4	35.6
Fe_2O_3	0.1	12.5	–	–	–	–	−7	0.05	−6.1	46.2

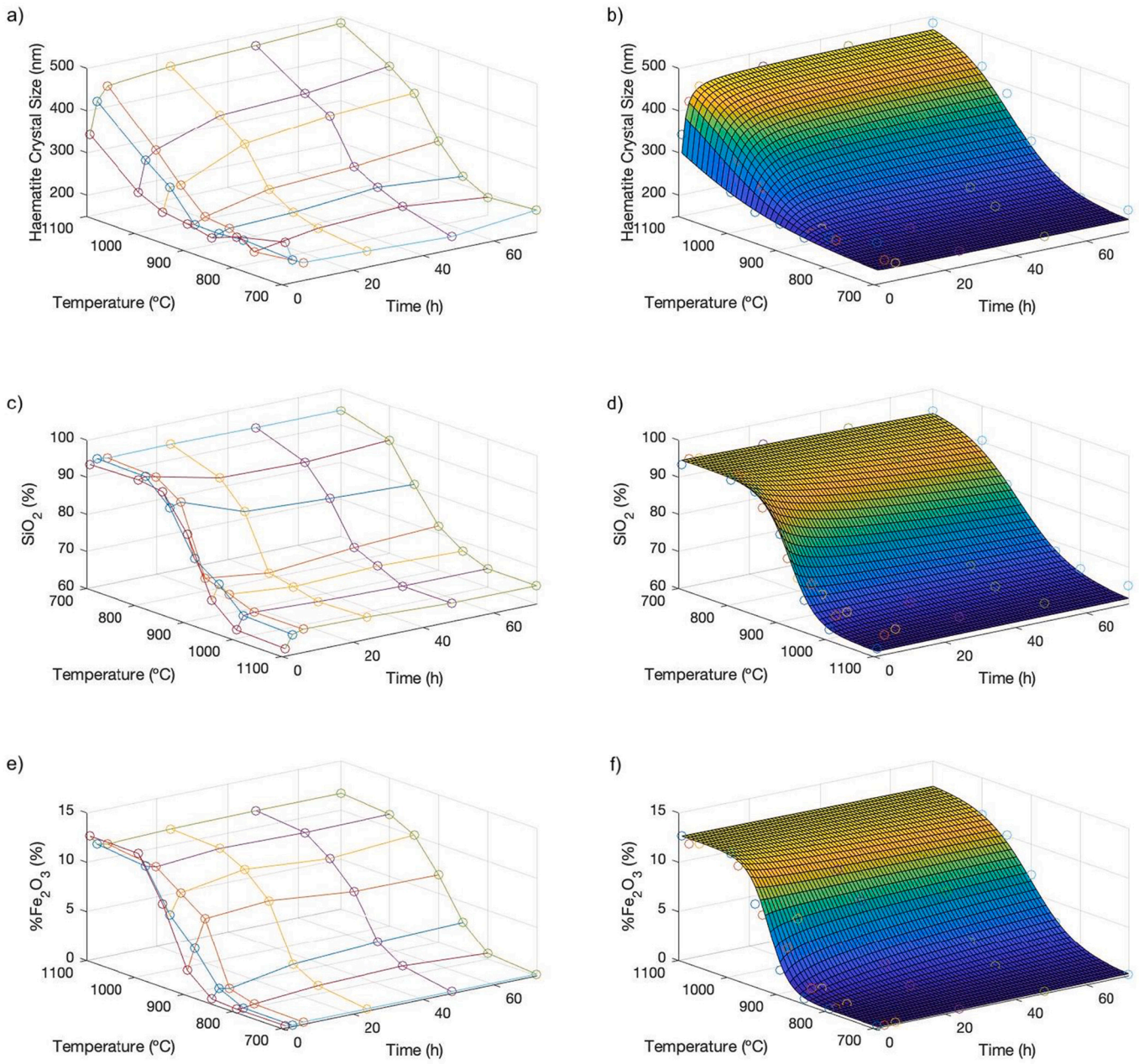

Fig. 9. (a, c, e) Three-dimensional representation of the experimental results obtained for the selected analytical variables (HCS, % SiO_2, and % Fe_2O_3) depending on firing temperatures and times. (b, d, f) Three-dimensional representation of the experimental model obtained with Eq. (1), their two variants (Eqs. (2) and (3)) and the constants presented in Table 4.

Table 5
Coefficient of determination (R^2) and mean difference percentage (± STD) between the model and experimental data of the linear regressions (Eqs. (6)–(11)) for each analytical variable used.

	First regression		Second and third regression		
Variable	R_1^2	Δ%Var ± STD	R_2^2	R_3^2	Δ%Var ± STD
HCS	0.96 ± 0.03	−1.7% ± 5.3%	0.98	0.85	−1.7% ± 6.1%
%SiO_2	0.93 ± 0.04	−0.2% ± 8.5%	0.95	0.95	−0.1% ± 8.5%
%Fe_2O_3	0.96 ± 0.02	0.6% ± 7.3%	0.83	0.84	0.8% ± 7.6%

obtaining the best mechanical properties.

4. Conclusions

The firing conditions of the unique *carreaux de pavement* found in the Iberian Peninsula were determined by comparing the physicochemical and mineralogical properties of the archaeological tiles with those of some *replicas* manufactured in the laboratory and heated at different times and temperatures. The replication of the firing conditions of archaeological ceramic samples through experimental archaeology made it possible to establish a range of firing temperatures of 875 to 950 °C. Likewise, the firing time was determined to be longer than 24 h.

To obtain these results, the changes in the haematite crystal size and the composition of the acid digestion residue (% SiO_2 and % Fe_2O_3) were determined, and an experimental model was created that considered

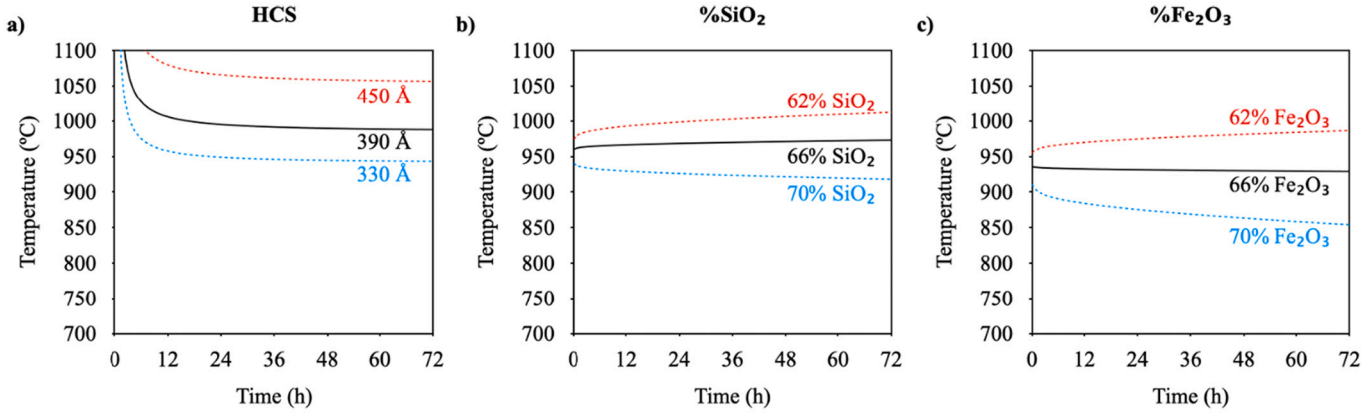

Fig. 10. Temperature–time curves for the manufacture of archaeological tiles. Red, maximum values; blue, minimum values; and black, mean values. (For interpretation of the references to colour in this figure legend, the reader is referred to the web version of this article.)

Table 6
Firing time and temperature in bibliographical sources.

Reference	Site	Thickness (cm)	Temperature (°C)	Time (h)	Atmosphere	Experimental basis
Norton, 1992	France	–	1.000	48	Oxidant	Glaze melting
Ben Amara et al., 2005	Bourges	1.5–2.0	850–900	–	Oxidant	Presence of gehlenite
Cicuttini et al., 2007	Aquitanie	1.9–2.6	Above 800	–	Oxidant	Glaze melting
Leon et al., 2007	Aquitanie	2.3	–	–	Oxidant	–
Cicuttini et al., 2008	Aquitanie	–	Above 800	–	Oxidant	Glaze melting
Métreau et al., 2012	Bretagne	2.3–2.7	–	–	Oxidant	–
Rouzeau et al., 2013	Langres	2.0–3.0	–	–	Oxidant	–

firing temperatures, times and the aforementioned analytical variables. The determination of the minimum firing times was also possible thanks to the identification of hercynite inside the samples fired at times <24 h, which was not present in the archaeological samples.

Two types of *replicas* were manufactured: CU samples for studying the inner parts of the bodies and QP sample for studying the surface. The thickness of the samples was a relevant factor since the interior suffers a delay with respect to the surface in the firing temperature changes, as well as a different effect of the surrounding atmosphere.

The firing temperature values provided in the literature (800–1000 °C), despite not being based on experimental data, are similar to those obtained experimentally in this article. The temperature range provided by this new publication is much narrower and more precise. The literature estimates that the heating time was at least two days, which is compatible with the results obtained experimentally for the *replicas* (>24 h).

The firing conditions determined by using the model coincided with the greatest compressive strength (50 and 80 MPa).

The precise firing conditions used to produce *carreaux de pavement* bodies were revealed thanks to this study. These firing data are the most accurate that have been obtained for *carreaux de pavement* and will serve as a basis for future research. The analytical techniques and numerical methods developed in this publication will serve as a model to apply to other ceramic materials whose firing conditions are to be known.

CRediT authorship contribution statement

Iván Ruiz-Ardanaz: Conceptualization, Methodology, Writing – original draft, Data curation, Software, Funding acquisition. **Marta Gil-Fernández:** Methodology, Data curation. **Esther Lasheras:** Conceptualization, Methodology, Writing – review & editing, Project administration, Funding acquisition. **Adrián Durán:** Conceptualization, Methodology, Writing – review & editing, Supervision, Project administration, Funding acquisition.

Declaration of Competing Interest

The authors declare that they have no known competing financial interests or personal relationships that could have appeared to influence the work reported in this paper.

Data availability

Data will be made available on request.

Acknowledgements

The reported study was funded by the Dirección General de Cultura-Institución Príncipe de Viana (Navarre Government) under the projects "Thibalt. Caracterización arqueométrica de Carreaux de Pavement procedentes del Castillo de Tiebas (Navarra)" and "Aplicación del arqueomagnetismo y otras técnicas fisicoquímicas para el estudio de la tecnología de fabricación de azulejos medievales navarros". I.R.-A. also acknowledges the Asociación de Amigos de la Universidad de Navarra for his doctoral grant. The authors wish to thank the staff from the Chemistry Department of the University of Navarra.

Appendix A. Supplementary data

Supplementary data to this article can be found online at https://doi.org/10.1016/j.clay.2022.106725.

References

Amicone, A., Forte, V., Soulard, B., Berthold, C., Memmesheimer, A., Mirkovíc-Maríc, N., 2021. Playing with fire: exploring ceramic pyrotechnology in the late Neolithic Balkans through an archaeometric and experimental approach. J. Archaeol. Sci. Rep. 37, 102878 https://doi.org/10.1016/j.jasrep.2021.102878.

Aras, A., 2004. The change of phase composition in kaolinite- and illite-rich clay-based ceramic bodies. Appl. Clay Sci. 24, 257–269. https://doi.org/10.1016/j.clay.2003.08.012.

Baccour, H., Medhioub, M., Jamoussi, F., Mhiri, T., 2009. Influence of firing temperature on the ceramic properties of Triassic clays from Tunisia. J. Mater. Process. Technol. 209, 2812–2817. https://doi.org/10.1016/j.jmatprotec.2008.06.055.

Backes, C.J., Cheetham, J.D., Neff, H., 2012. The Color of Influence: A Provenance Study of Hematite-Based Paints on Early Olmec Carved Pottery, 23. Cambridge University Press, pp. 70–92. https://doi.org/10.7183/1045-6635.23.1.70.

Barbie, M., Cailleaux, D., Chapelot, O., 1987. Carreaux de Pavement du Moyen Âge et de la Renaissance. Catalogue des collections des Musées de Chaumont et de Saint-Dizier (Haute-Marne), Chaumont.

Ben Amara, A., Gourdon-Platel, N., Bechtel, F., Schwoerer, M., Bon, P., 2005. Carreaux glaçurés provenant d'un château du Duc de Berry (Mehun-sur-Yèvre, fin XIV siècle): recherche d'indices techniques. ArcheoSciences. 29, 21–34. https://doi.org/10.4000/archeosciences.441.

Bratitsi, M., Liritzis, I., Vafiadou, A., Xanthopoulou, V., Palamara, E., Iliopoulos, I., Zacharias, N., 2018. Critical assessment of chromatic index in archaeological ceramics by munsell and RGB: novel contribution to characterization and provenance studies. Mediter. Archaeol. Archaeom. 18, 175–212. https://doi.org/10.5281/zenodo.1297163.

Busuttil, C., 2013. Experimental archaeology. Malta Archaeol. Rev. 9, 60–66.

Castiella, A., 1998. Informe sobre los trabajos arqueológicos realizados en el Castillo de Tiebas (Navarra). Trabajos de Arqueología Navarra 13, 247–286.

Chen, C.Y., Lan, G.S., Tuan, W.H., 2000. Microstructural evolution of mullite during the sintering of kaolin powder compacts. Ceram. Int. 26, 715–720. https://doi.org/10.1016/S0272-8842(00)00009-2.

Cicuttini, B., 2012. Les carreaux estampés bicolores du sud-ouest de la France. Presses universitaires François-Rabelais, Tours, pp. 309–319. https://doi.org/10.4000/books.pufr.7357.

Cicuttini, B., Merat, A., Ben Amara, A., Bechtel, F., 2007. Étude stylistique et technologique des carreaux de pavement du château de Lormont (Gironde, XIII - XIV siècles). In: Actes du 4ème Congrès international d'Archéologie Médiévale et Moderne, 3. París, hal-01983251.

Cicuttini, B., Ben Amara, A., Bechtel, F., 2008. An Investigation into the Ceramic Technology of the Two-Colour Tiles of "Prince Noir" Castle (Bordeaux, France, Thirteenth to Fourteenth Centuries AD). In: Proceedings of the 37th International Symposium on Archaeometry, pp. 55–60. Siena. https://doi.org/10.1007/978-3-642-14678-7_.

Cultrone, G., Sebastian, E., Elert, K., de la Torre, M.J., Cazalla, O., Rodriguez Navarro, C., 2004. Influence of mineralogy and firing temperature on the porosity of bricks. J. Eur. Ceram. Soc. 13, 621–634. https://doi.org/10.1016/S0955-2219(03)00249-8.

Daghmehchi, M., Rathossi, C., Omrani, H., Emami, M., Rahbar, M., 2018. Mineralogical and thermal analyses of the Hellenistic ceramics from T Laodicea Temple, Iran. Appl. Clay Sci. 162, 146–154. https://doi.org/10.1016/j.clay.2018.06.007.

De Benedetto, G.E., Laviano, R., Sabbatini, S., Zambonin, P.G., 2002. Infrared spectroscopy in the mineralogical characterization of ancient pottery. J. Cult. Herit. 3, 177–186. https://doi.org/10.1016/S1296-2074(02)01178-0.

De Bonis, A., Cultrone, G., Grifa, C., Langella, A., Leone, A.P., Mercurio, M., Morra, V., 2017. Different shades of red: the complexity of mineralogical and physico-chemical factors influencing the colour of ceramics. Ceram. Int. 43, 8065–8074. https://doi.org/10.1016/j.ceramint.2017.03.127.

De Los Arcos, T., Müller, H., Wang, F., Damerla, V.R., Hoppe, C., Weinberg, C., Tiemann, M., Grundmeier, G., 2021. Review of infrared spectroscopy techniques for the determination of internal structure in thin SiO2 films. Vib. Spectrosc. 114, 103256 https://doi.org/10.1016/j.vibspec.2021.103256.

Encyclopaedia of Global Archaeology (EGA), 2022. https://link.springer.com/referenceworkentry/10.1007%2F978-1-4419-0465-2_360 accessed 24 March.

Gómez-Castañedo, A., 2005. Arqueología experimental como herramienta de divulgación científica. In: El ejemplo del Grupo Arqueológico ATTICA. Conferencia Arqueología Experimental en la Península Ibérica. Santander.

González-Martí, M., 1952. Cerámica del Levante Español - Siglos Medievales - Tomo III. Azulejos, socarrats y retablos. Editorial Labor, Barcelona, 1952.

Grassi, F., Quirós-Castillo, J.A., 2018. Arqueometría de los Materiales Cerámicos de Época Medieval en España: Arqueometría y arqueología de la cerámica medieval en España. Balance crítico y perspectivas de futuro. Documentos de Arqueología Medieval 12, 23–38.

Ingersoll, D., Yellen, J.E., Macdonald, W., 1977. Experimental Archaeology. Columbia University press, New York.

Jordán, M.M., Boix, A., Sanfeliu, T., de la Fuente, C., 1999. Firing transformations of cretaceous clays used in the manufacturing of ceramic tiles. Appl. Clay Sci. 14, 225–234. https://doi.org/10.1016/S0169-1317(98)00052-0.

Jordanova, N., Jordanova, D., Barrón, V., Lesigyarski, D., Kostadinova, M., 2019. Rock-magnetic and color characteristics of archaeological samples from burnt clay from destructions and ceramics in relation to their firing temperature. Archaeol. Anthropol. Sci. 11, 3595–3612. https://doi.org/10.1007/s12520-019-00782-y.

Karaman, S., Ersahin, S., Gunal, H., 2006. Firing temperature and firing time influence on mechanical and physical properties of clay bricks. J. Sci. Ind. Res. 65, 153–159.

Legodi, M.A., de Waal, D., 2007. Raman spectroscopic study of ancient South African domestic clay pottery. Spectrochim. Acta A 66, 135–142. https://doi.org/10.1016/j.saa.2006.02.059.

Leon, Y., Ben Amara, A., Conte, P., 2007. Carreaux de pavement glaçurés du château du Haut Châlucet (Haute-Vienne, XIII - XIV s.) - Inventaire et techniques de fabrication. In: Actes du 4ème Congrès international d'Archéologie Médiévale et Moderne, 45, pp. 131–152.

Majer, J., 1995. Mathematical approximation of sigmoidal shape curves tested on sensitometric curves of photographic material. J. Chemom. 9, 59–66. https://doi.org/10.1002/cem.1180090106.

Maritan, L., Nodari, L., Olivieri, L.M., Vidale, M., 2020. Shades of black: production technology of the black slip ware from Barikot, North-Western Pakistan. J. Cult. Herit. 43, 342–355. https://doi.org/10.1016/j.culher.2019.10.002.

Martínez, D., Ruiz, F.J., Vallejo, J.M., 2011. Algunas consideraciones en torno a unas baldosas góticas decoradas y vidriadas aparecidas en la ermita de Santa Catalina en Tiebas (Navarra). Trabajos de Arqueología Navarra 23, 141–160. https://revistas.navarra.es/index.php/TAN/article/view/113.

Martín-Márquez, J., Rincón, J.M., Romero, M., 2008. Effect of firing temperature on sintering of porcelain stoneware tiles. Ceram. Int. 34, 1867–1873. https://doi.org/10.1016/j.ceramint.2007.06.006.

Măruţoiu, C., Bratu, I., Ţiplic, M.I., Măruţoiu, V.C., Nemeş, O.F., Neamţu, C., Hernanz, A., 2018. FTIR analysis and 3D restoration of Transylvanian popular pottery from the XVI-XVIII centuries. J. Archaeol. Sci. Rep. 19, 148–154. https://doi.org/10.1016/j.jasrep.2018.02.044.

Mayer, J., Garrigou, P., 2000. Pavement. In: Carreaux de sol en Champagne au Moyen-Âge et à la Renaissance, 4. Editions du Patrimoine, París, pp. 393–394.

MDHS101, 2005. Measurement of Quartz in Respirable Airborne Dust by Infrared Spectroscopy and X-Ray Diffractometry.

Medeghini, L., Mignardi, S., De Vito, C., Conte, A.M., 2016. Evaluation of a FTIR data pretreatment method for principal component analysis applied to archaeological ceramics. Microchem. J. 125, 224–229. https://doi.org/10.1016/j.microc.2015.11.033.

Métreau, L., Cantin, N., Bechtel, F., Rosen, J., André, P., 2012. De Suscinio I à Suscinio II : rupture ou continuité ? Étude archéométrique des carreaux décorés à glaçure transparente des pavements médiévaux du château de Suscinio (Sarzeau, Morbihan). Revue archéologique de l'Ouest 29, 243–249.

Montero, I., García, M., López-Romero, E., 2007. Arqueometría: cambios y tendencias actuales. Trab. Prehist. 64, 23–40. https://doi.org/10.3989/tp.2007.v64.i1.92.

Moses, I.J., Ben, E., 2018. The effect of holding time on the compressive strength of Mukono Ntawo ball clay. Int. J. Innov. Sci. Res. Technol. 3, 281–288.

Nodari, L., Marcuz, E., Maritan, L., Mazzoli, M., Russo, U., 2007. Hematite nucleation and growth in the firing of carbonate-rich clay for pottery production. J. Eur. Ceram. Soc. 27, 4665–4673. https://doi.org/10.1016/j.jeurceramsoc.2007.03.031.

Noghani, S., Emami, M., 2014. Mineralogical phase transition on sandwich-like structure of clinky pottery from Parthian period, Iran. Periodico di Mineralogia 83, 171–185. https://doi.org/10.2451/2014pm0010.

Norton, C., 1992. Carreaux De Pavement Du Moyen Âge Et De La Renaissance: Collections Du Musée Carnavalet. Editions Paris-Musées, París.

Pérez-Monserrat, E.M., Cultrone, G., Rincón, J.M., Perla, A., Fort, R., 2019. Multidisciplinary study of glazed ceramics from Chamberí Metro station (Madrid, Spain): a knowledge base with technological and heritage value. Appl. Clay Sci. 175, 102–114. https://doi.org/10.1016/j.clay.2019.03.032.

Perrin, J.F., 2005. Bibliothèque des Génies et des Fées, 12, pp. 382–383. https://doi.org/10.4000/feeries.175.

Ramis-Ramos, G., Álvarez-Coque, M.C., 2001. Quimiometría. Editorial Síntesis, Madrid.

Ramos, M., 2001. Excavaciones en el castillo de Tiebas (Navarra), primer informe provisional, 1998. Trabajos de Arqueología Navarra 15, 167–213.

Ramos, M., 2004. La arqueología experimental para una mejor interpretación de los datos en arqueología histórica. Anuario de Arqueología 12, 73–104.

Ramos, M., 2009. Descubrimiento de un pavimento de baldosas decoradas en el castillo-palacio de Tiebas. Trabajos de Arqueología de Navarra 21, 317–324.

Rouzeau, B., Bocquet-Liénard, A., Moulis, C., 2013. Les carreaux de pavement découverts à l'abbaye de Morimond (Haute-Marne): étude typologique, technique et archéométrique. Revue archéologique de l'Est 62 (185), 343–366. http://rae.revues.org/7852.

Ruiz-Ardanaz, I., Lasheras, E., Durán, A., 2021. Mineralogical Characterization of *Carreaux de Pavement* from Northern Spain (Tiebas, Navarre). Minerals 11 (153). https://doi.org/10.3390/min11020153.

Ruiz-Ardanaz, I., Lasheras, E., Durán, A., 2023. Determination of the Place of Production of the Carreaux de Pavement of the Castle of Tiebas by Means of Physicochemical Methods. [Unpublished Manuscript, in Process].

Thér, R., Kallistová, A., Svoboda, Z., Květina, P., Lisá, L., Burgert, P., Bajer, A., 2019. How was neolithic pottery fired? An exploration of the effects of firing dynamics on ceramic products. J. Archaeol. Method Theory 26, 1143–1175. https://doi.org/10.1007/s10816-018-9407-x.

Tite, M.S., 1969. Determination of the firing temperature of ancient ceramics by measurement of thermal expansion: a reassessment. Archaeometry 11, 131–143. https://doi.org/10.1111/j.1475-4754.1969.tb00636.x.

Tite, M.S., Kilikoglou, V., Vekinis, G., 2003. Strength, toughness and thermal shock resistance of ancient ceramics, and their influence on technological choice. Archaeometry 43, 301–324. https://doi.org/10.1111/1475-4754.00019.

Torrent, J., Barrón, V., 2003. The visible diffuse reflectance spectrum in relation to the color and crystal properties of hematite. Clay Clay Miner. 51, 309–317. https://doi.org/10.1346/ccmn.2003.0510307.

Torrent, J., Schwertmann, U., Fechter, H., Alferez, F., 1983. Quantitative relationships between soil color and hematite content. Soil Sci. 136, 354–358. https://doi.org/10.1097/00010694-198312000-00004.

Traoré, K., Kabré, T.S., Blanchart, P., 2003. Gehlenite and anorthite crystallisation from kaolinite and calcite mix. Ceram. Int. 29, 377–383. https://doi.org/10.1016/s0272-8842(02)00148-7.

Xiong, R., Xie, G., Edmondson, A.E., Sheard, M.A., 1999. A mathematical model for bacterial inactivation. Int. J. Food Microbiol. 46, 45–55. https://doi.org/10.1016/s0168-1605(98)00172-x.

Yin, X., Goudriaan, J.A.N., Lantinga, E.A., Vos, J.A.N., Spiertz, H.J., 2003. A flexible sigmoid function of determinate growth. Ann. Bot. 91, 361–371. https://doi.org/10.1093/aob/mcg029.

Zullinger, E.M., Ricklefs, R.E., Redford, K.H., Mace, G.M., 1984. Fitting sigmoidal equations to mammalian growth curves. J. Mammal. 65, 607–636. https://doi.org/10.2307/1380844.